Article

Rhodium and Hafnium Influence on the Microstructure, Phase Composition, and Oxidation Resistance of Aluminide Coatings

Maryana Zagula-Yavorska *, Małgorzata Wierzbińska and Jan Sieniawski

Department of Materials Science, Rzeszow University of Technology, W. Pola 2 str., 35-959 Rzeszow, Poland; mwierzb@prz.edu.pl (M.W.); jansien@prz.edu.pl (J.S.)

* Correspondence: yavorska@prz.edu.pl; Tel.: +48-17-865-1230

Abstract: A 0.5 μm thick layer of rhodium was deposited on the CMSX 4 superalloy by the electroplating method. The rhodium-coated superalloy was hafnized and aluminized or only aluminized using the Chemical vapour deposition method. A comparison was made of the microstructure, phase composition, and oxidation resistance of three aluminide coatings: nonmodified (a), rhodium-modified (b), and rhodium- and hafnium-modified (c). All three coatings consisted of two layers: the additive layer and the interdiffusion layer. Rhodium-doped (rhodium- and hafnium-doped) β-NiAl phase was found in the additive layer of the rhodium-modified (rhodium- and hafnium-modified) aluminide coating. Topologically Closed-Pack (μ and σ) phases precipitated in the matrix of the interdiffusion layer. Rhodium also dissolved in the β-NiAl phase between the additive and interdiffusion layers, whereas Hf-rich particles precipitated in the (Ni,Rh)Al phase at the additive/interdiffusion layer interface in the rhodium- and hafnium-modified coating (c). The rhodium-modified aluminide coating (b) has better oxidation resistance than the nonmodified one (a), whereas the rhodium- and hafnium-modified aluminide coating (c) has better oxidation resistance than the rhodium-modified (b) and nonmodified (a) ones.

Keywords: rhodium; hafnium; aluminide coating; CMSX 4 superalloy; oxidation

1. Introduction

Extending the lifetime of turbine blades is a continuous problem for aircraft engine manufacturers. According to Beranoagirre et al. [1], turbine blades and compressor blades could be manufactured from γ-TiAl alloys, but high hardness and machining problems have limited their usage in the aerospace industry.

Developments in alloy design and reliable thermal barrier coating systems deposited on superalloys have been used to increase the lifetime of turbine blades. Nickel aluminide intermetallic coatings are used in the thermal barrier coatings between the ceramic topcoat and the superalloy substrate. The melting point of nickel aluminides is about 1640 °C, so aluminides are used as oxidation-resistant coatings with good thermal stability for high temperature applications [2]. The oxidation resistance of the uncoated and aluminized nickel-base single-crystal superalloy was investigated at 900 °C for 500 h [3]. The better oxidation resistance of coated superalloys was due to the phase transformation from θ-Al_2O_3 to α-Al_2O_3 with increasing oxidation time. The oxidation behavior of aluminized CM186LC single-crystal superalloy was also investigated between 900 °C and 1100 °C [4]. It was found that aluminide coatings improved the oxidation resistance of the superalloy. The mass gain of specimens after 100 h of oxidation decreased through phase transformation of θ-Al_2O_3 to α-Al_2O_3 and growth of stable α-Al_2O_3 oxide.

Aluminide coatings were produced on the Ni–18Fe–17 Cr superalloy and oxidized at 1000 °C for 200 h [5]. A dense and slow-growing α-Al$_2$O$_3$ oxide that protects the superalloy substrate from oxidation was found [5]. The aluminizing process greatly enhances the oxidation resistance of Hastelloy X at 1100 °C due to a dense and protective alumina layer formed during oxidation [6]. Although aluminide coatings contain enough aluminum to form aluminum oxide during oxidation, its adherence is poor [7]. Platinum modification improves aluminum oxide adherence to the coatings [7]. Benoist et al. [7] produced a platinum layer (5 and 10 μm thick) on the IN 100 and AM 1 superalloys using the electrodeposition method. Then, heat treatment was performed to enable platinum diffusion into the substrate, and aluminizing was then performed. Purvis et al. [8] produced a platinum layer (4, 7, 11 and 14 μm thick) on the IN 100, Mar 247, and PWA 1480 superalloys by electrodeposition and aluminizing was then performed. Wang et al. [9] produced a platinum layer (4–7 μm thick) on the Haynes 188 and WI-52 superalloys by electrodeposition. After the electroplating process, samples were heat treated in a vacuum at 1052 °C for 1 h. Then, aluminizing was performed. Zagula-Yavorska et al. [10] produced a platinum layer (3 and 7 μm thick) on the In 713 LC, In 625, and CMSX 4 superalloys by electrodeposition. Afterwards, the samples were diffusion-treated and aluminized. The microstructure and phase composition of platinum-modified aluminide coatings depend on platinum layer thickness as well as the methods and parameters of aluminizing [11]. The PtAl$_2$, β-(Ni,Pt)Al, or β-(Ni,Pt)Al + PtAl$_2$ phases may be formed [11]. The β-(Ni,Pt)Al phase coatings containing 15–20 wt % aluminum and 20–25 wt % platinum are less brittle than coatings consisting of β-(Ni,Pt)Al + PtAl$_2$ phases [11].

Platinum improves the oxidation resistance of coatings via different mechanisms. Platinum lowers the activity of aluminum in nickel aluminide coatings. Gleeson et al. [12] suggested that platinum accumulates near the thermally grown oxide due to the selective oxidation of other elements. Then, the aluminum activity gradient is increased, and the flux of aluminum to the thermally grown oxide/intermetallic coating interface is increased as well. This phenomenon promotes alumina scale formation. Platinum reduces the speed of the oxide layer formation and favors formation of pure alumina oxide. Moreover, the NiAl phase is stabilized and NiAl–Ni$_3$Al transformation is prevented [13]. According to Haynes et al. [14], platinum modification not only improves aluminum oxide adherence to the coatings during oxidation, but also decreases the harmful influence of sulfur and lowers the void content at the oxide/coating interface. According to Zagula-Yavorska et al. [10], platinum favors the formation of pure Al$_2$O$_3$ oxide, retards Al$_2$O$_3$ oxide spallation, and inhibits aluminide coating degradation. However, poor high cyclic fatigue performance of platinum-modified aluminide coatings requires replacing the platinum in the coatings by other metal [15]; for instance, hafnium. Research on hafnium-doped cast alloys has indicated that hafnium in β-NiAl and Ni–Pt aluminides reduces the parabolic rate constant of oxidation by a factor of ten and is more efficient than platinum [16]. Hafnium has a high affinity to oxygen [17]. The addition of a small hafnium content (<1 wt %) to the aluminide coatings causes the formation of pegs during oxidation, and thus improves the oxidation resistance of coated superalloys [18].

Rhodium addition to the hot-rolled Ni–8Cr–6Al alloys has been investigated as an alternative to platinum [19]. It was found that addition of 5 wt % rhodium to the Ni–8Cr–6Al alloy is approximately equivalent to 10 wt % platinum. Rhodium increases Al$_2$O$_3$ adherence to the Ni–8Cr–6Al alloy and improves its oxidation resistance. Rhodium-modified aluminide coatings show better oxidation resistance than nonmodified ones [20].

To improve the lifetime of aluminide coatings, rhodium- and hafnium-modified aluminide coatings need to be produced. Therefore, the aim of this paper was the analysis of the effect of rhodium and of rhodium and hafnium on the microstructure, phase composition, and oxidation resistance of aluminide coatings deposited on the CMSX 4 superalloy. The microstructure, phase composition, and oxidation resistance of rhodium-modified and rhodium- and hafnium-modified aluminide coatings were compared with nonmodified ones. Until now, such investigations have not been performed.

2. Experimental Procedure

The cylindrical samples made of CMSX 4 superalloy (monocrystal) were cut and ground up to SiC No 1000, degreased in ethanol, ultrasonically cleaned, and finally coated with a rhodium layer (0.5 µm thick). The chemical composition of the CMSX 4 superalloy is presented in Table 1. The rhodium layer was deposited using the electroplating method.

The rhodium electroplating process was conducted in a bath of rhodium sulphate $Rh_2(SO_4)_3$ (0.1 g/dm^3) (Alchem, Rzeszow, Poland), sulphuric acid H_2SO_4 (0.15 g/dm^3) (Alchem, Rzeszow, Poland), and selenium acid H_2SeO_4 (0.010g/dm^3) (Alchem, Rzeszow, Poland) at 50 °C. The current density during the electroplating process was about 0.2 A/dm^2. After electroplating, samples were cleaned in water heated to 70 °C.

Then, the aluminide coatings were deposited using the CVD equipment BPXPR0325S (IonBond Company, Olten, Switzerland) [21–23]. Aluminum chloride vapor (AlCl$_3$) was produced in an external generator I (IonBond Company, Olten, Switzerland) at 330 °C as a result of hydrogen chloride flow (0.2 L/min) via aluminum granules. Then, AlCl$_3$ was transported in a stream of hydrogen into the CVD reactor (IonBond Company, Olten, Switzerland), where samples were placed. Hafnium chloride vapor (HfCl$_3$) was produced in an external generator II (IonBond Company, Olten, Switzerland) at about 400 °C as a result of hydrogen chloride flow via hafnium granules. Then, HfCl$_3$ was transported in a stream of hydrogen gas into the CVD reactor.

The rhodium-coated samples were hafnized and aluminized by the CVD method in the following stages:

I. heating from room temperature up to 1040 °C;
II. hafnizing with aluminizing at 1040 °C for 360 min;
III. aluminizing at 1040 °C for 360 min;
IV. cooling samples with the furnace.

Several samples were aluminized with pre-deposited rhodium layers by the CVD method at 1050 °C for 12 h.

Table 1. Chemical composition of the CMSX 4 superalloy, wt %.

Ni	Cr	Mo	Nb	Ta	Al	Ti	Co	W	Hf	Re
61.7	6.5	0.6	-	6.5	5.6	1	9	6	0.1	3

Nonmodified aluminide coatings were also deposited. The rhodium-modified (b) as well as nonmodified (a) and hafnium- and rhodium-modified (c) aluminide coatings were oxidized in an air atmosphere at 1100 °C. Samples were placed in the furnace and heated to 1100 °C, then removed from the furnace after 20 h and cooled in the air atmosphere to room temperature. Specimens were weighed and inspected after each cycle of oxidation. Microstructure, chemical, and phase composition of coatings were determined using scanning electron microscopy (SEM) (Hitachi America, Ltd., Iowa City, IA, USA), energy dispersive spectroscopy (EDS) (Hitachi America, Ltd., Iowa City, IA, USA), and X-ray diffraction (XRD) (XTRa ARL, Waltham, MA, USA).

3. Results

3.1. Nonmodified Aluminide Coatings (a)

The surface of the nonmodified coating consists of polyhedral-shaped grains (Figure 1a). The grain size on the surface is about 6–20 µm. The core and grain boundary consist of nickel, aluminum, cobalt, and chromium (Figure 1b,c). The overall surface chemical composition is 51.0Al–44.7Ni–0.6Cr–3.7Co (atom %). This indicates the presence of the Al-rich β-NiAl phase. Microstructure analysis on the cross-section revealed that the coating is composed of two layers:

an additive layer and an interdiffusion layer (Figure 2). The total coating's thickness is about 30 μm (Figure 2a). The distribution of Ni and Al in the cross-section confirms the presence of the β-NiAl phase (Figure 2b). The NiAl phase peaks of nonmodified aluminide coatings are shifted to bigger diffraction angles in comparison with standard β-NiAl phase peaks (Figures 3 and 4). This is probably due to incorporation of chromium and/or cobalt to the β-NiAl phase. The interdiffusion layer and the substrate/interdiffusion interface are rich in inclusions containing alloying elements. The analysis of the chemical composition of these phases suggests the presence of Topologically Closed-Pack μ and σ phases. TEM analysis confirmed the presence of μ and σ Topologically Closed-Pack phases [24].
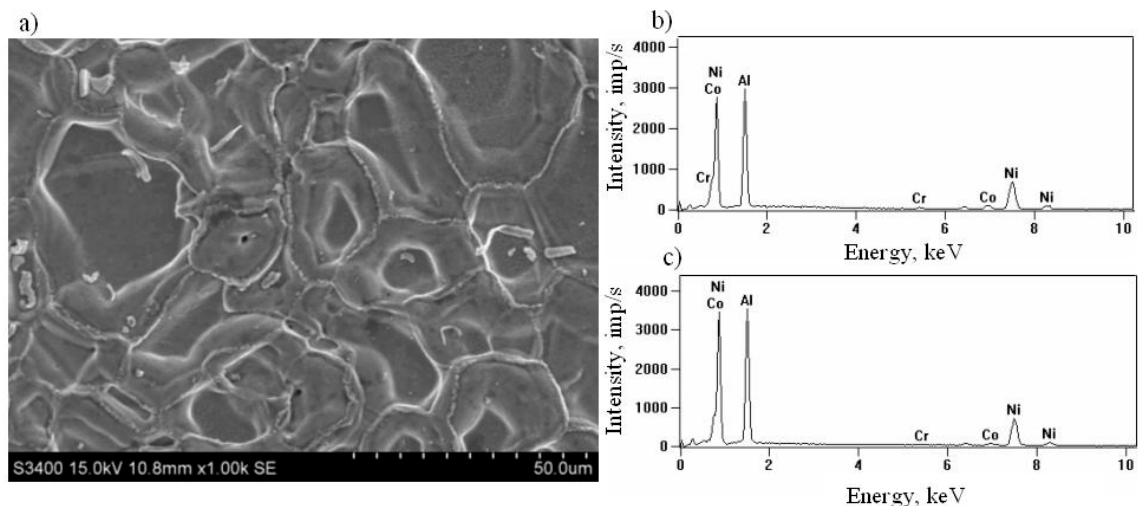
Figure 1. Surface morphology (**a**), Energy Dispersive Spectrum EDS of grain core (**b**), and EDS spectrum of grain boundary (**c**) of the nonmodified aluminide coating.
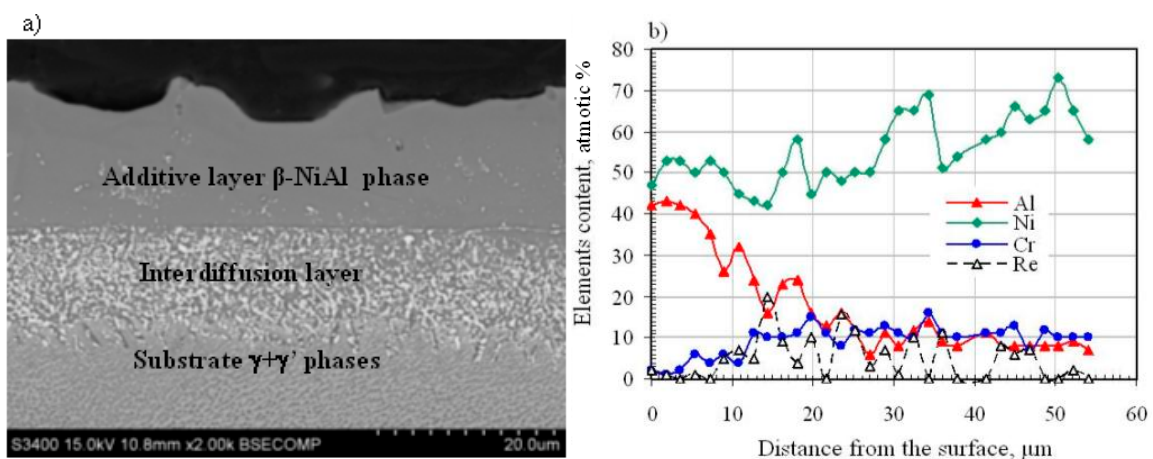
Figure 2. Microstructure (**a**) and elements' distribution (**b**) on the cross-section of the nonmodified aluminide coating.
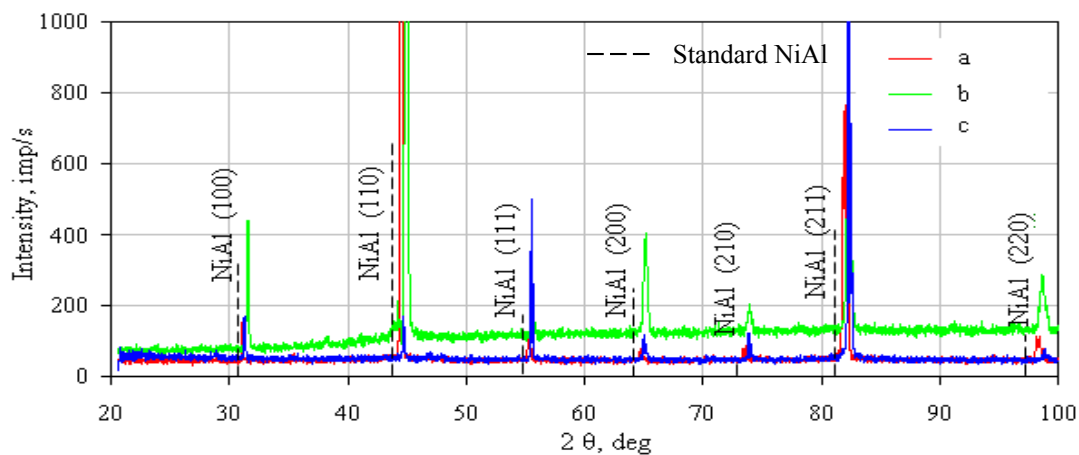
Figure 3. X-ray diffraction (XRD) patterns of the nonmodified (**a**), rhodium-modified (**b**) and rhodium- and hafnium-modified (**c**) aluminide coatings.
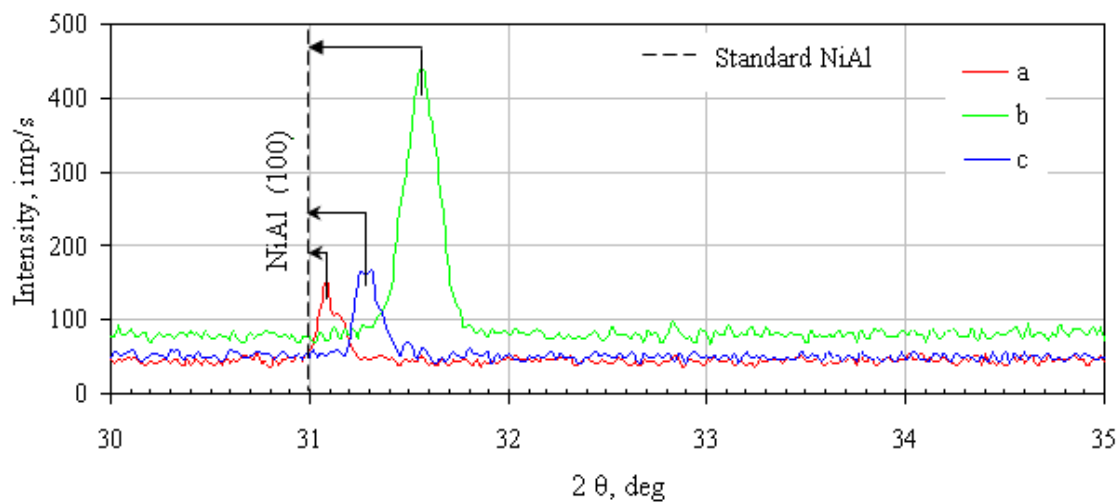
Figure 4. XRD shifts of the NiAl (100) reflection of the nonmodified (**a**), rhodium-modified (**b**) and rhodium- and hafnium-modified (**c**) aluminide coatings.

3.2. Rhodium-Modified Aluminide Coatings (b)

The surface of the rhodium-modified aluminide coating consists of polyhedral-shaped grains, similar to the nonmodified coating (a) (Figure 5a). Grain size on the surface is about 19–38 μm. The core and grain boundary consist of nickel, aluminum, cobalt, and chromium. Moreover, some rhodium peaks are visible (Figure 5b,c). The overall surface composition is 49.8Al–45.8Ni–0.7Cr–3.7Co (atom %). The rhodium content on the surface of the coating is smaller than 0.1 wt %. Such a chemical composition indicates that the rhodium-doped β-NiAl phase has formed. Microstructure analysis on the cross-section showed that the coating is composed of two layers: an additive layer and an interdiffusion layer (Figure 6a), like the nonmodified one (a). The total coating's thickness is about 30 μm (Figure 6a). The EDS analysis on the cross-section showed that the top, additive layer is composed of the rhodium-doped β-NiAl (atom %: 44.0Al–2.6Cr–53.0Ni–0.4Rh). XRD surface analysis revealed that peaks of the β-NiAl phase are shifted to bigger diffraction angles in comparison with standard β-NiAl phase peaks (Figures 3 and 4). This is probably due to incorporation of rhodium into the β-NiAl phase. Rhodium content between the additive and interdiffusion layers is low (2–5 atom %) (Figure 6b). No rhodium-rich particles were observed in the additive layer, only Kirkendall-like

porosity and few particles of Topologically Closed-Pack phases (Figure 6a). Topologically Closed-Pack phases μ and σ containing refractory elements were also observed in the interdiffusion layer.
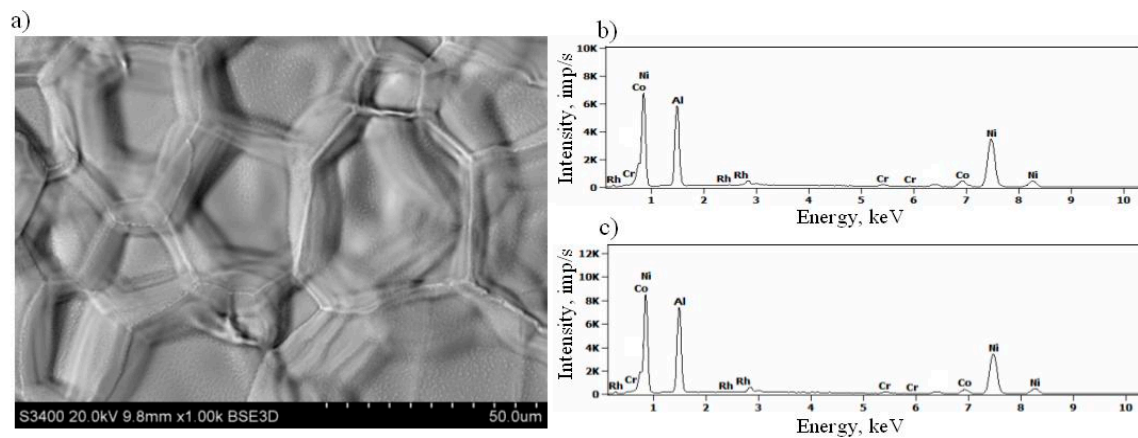
Figure 5. Surface morphology (**a**), EDS spectrum of grain core (**b**) and EDS spectrum of grain boundary (**c**) of the rhodium-modified aluminide coating.
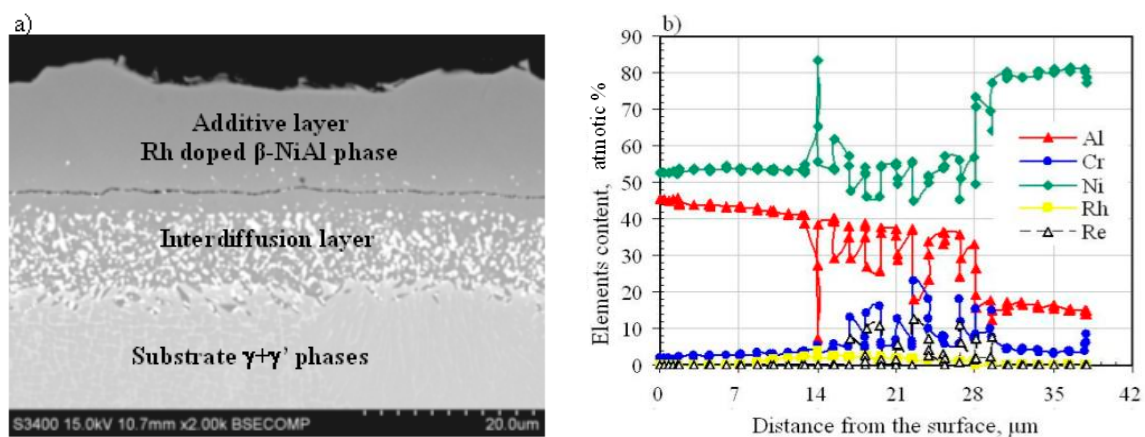
Figure 6. Microstructure (**a**) and elements' distribution (**b**) on the cross-section of the rhodium-modified aluminide coating.

3.3. Rhodium- and Hafnium-Modified Aluminide Coatings (c)

The surface of the rhodium- and hafnium-modified aluminide coating consists of polyhedral-shaped grains, similar to the nonmodified (a) and rhodium-modified (b) coatings (Figure 7a). Grain size on the surface is about 10–38 μm. The EDS analysis shows that the core and grain boundary consist of nickel, aluminum, cobalt, and chromium. Moreover, some rhodium and hafnium peaks are visible (Figure 7b,c). The overall surface composition is 48.1Al–46.6Ni–0.9Cr–4.4Co (atom %). The rhodium and hafnium content on the surface of the coating is less than 0.1 wt %. Microstructure analysis on the cross-section showed that, similarly to the nonmodified (a) and the rhodium-modified (b) coatings, the rhodium- and hafnium-modified (c) aluminide coating is composed of two layers: an additive one and an interdiffusion one (Figure 8a). The total coating's thickness is about 30 μm (Figure 8a). The EDS analysis on the cross-section showed that the top, additive layer is composed of the rhodium- and hafnium-doped β-NiAl phase (atom %: 43.0Al–0.8Cr–56.0Ni–0.1Rh–0.1Hf). XRD surface analysis revealed that peaks of β-NiAl phase are shifted to bigger diffraction angles in comparison with standard β-NiAl phase peaks (Figures 3 and 4). This is probably due to the incorporation of rhodium and hafnium into the β-NiAl. The rhodium content between the additive and interdiffusion layers is low (2–3 atom %). No rhodium-rich particles were observed in the additive

layer, only Kirkendall-like porosity (Figure 8a). Bright, hafnium-rich precipitates were observed at the additive/interdiffusion layer interface (Figure 8b, Table 2). Topologically Closed-Pack phases µ and σ containing refractory elements are visible in the interdiffusion layer. The elements' distribution on the cross-section of the coating indicates that hafnium is located at the additive/interdiffusion layer interface (Figure 9).
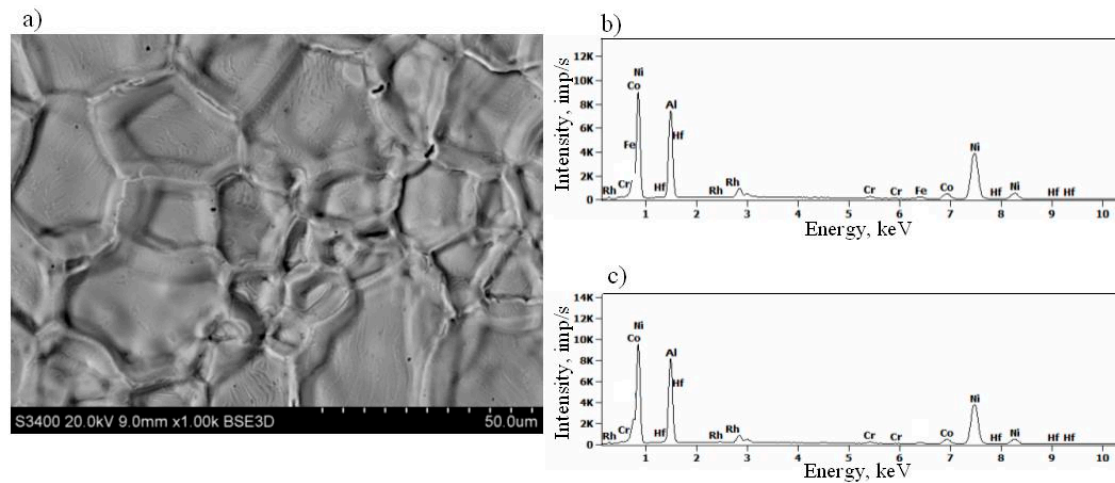
Figure 7. Surface morphology (**a**), EDS spectrum of grain core (**b**) and EDS spectrum of grain boundary (**c**) of the rhodium- and hafnium-modified aluminide coating.
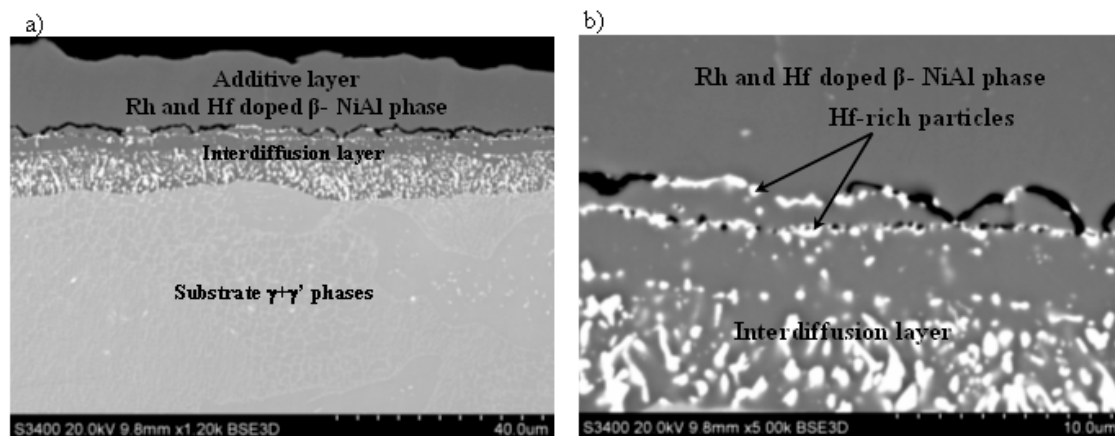
Figure 8. Microstructure on the cross-section of the rhodium- and hafnium-modified aluminide coating (**a**), hafnium-rich particles at the additive/interdiffusion layer interface (**b**).

Table 2. Chemical composition of the hafnium-rich particles.

Elements Content, atom %				
Al	Cr	Ni	Hf	Rh
39.1 ± 0.4	2.5 ± 0.1	54.1 ± 0.7	3.9 ± 0.3	0.4 ± 0.1
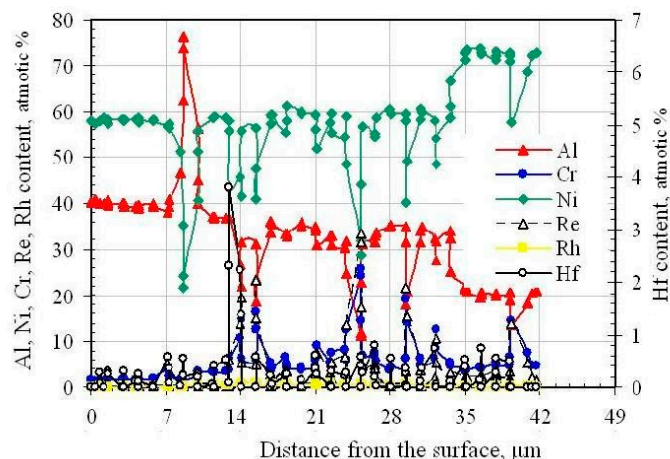
Figure 9. Elements' distribution on the cross-section of the rhodium- and hafnium-modified aluminide coating.

Both rhodium- (b) and rhodium-with-hafnium- (c) modified aluminide coatings show better oxidation resistance than the nonmodified one (a) (Figure 10).
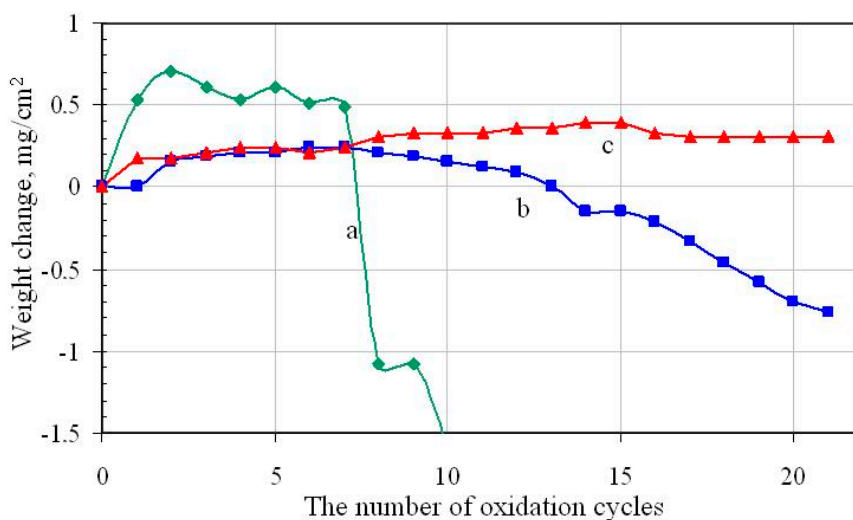
Figure 10. Oxidation test results of the nonmodified (**a**), rhodium-modified (**b**), rhodium- and hafnium-modified (**c**) aluminide coatings.

4. Discussion

The nonmodified aluminide coating's formation is a result of two processes [22]:

(1) diffusion of nickel, cobalt, chromium, titanium and other superalloys' elements from the substrate to the surface, leading to formation of the interdiffusion layer;

(2) reaction of nickel with aluminum supplied by the gas phase in the CVD process, and formation of the additive layer.

The total coating thickness includes two layers. Both of them consist of the β-NiAl phase. As the solubility of alloying elements in the β-NiAl phase is very low, these elements precipitate in Topologically Closed-Pack phases (μ and σ).

The rhodium content between the additive and interdiffusion layers is 5 atom %. According to the Al–Ni–Rh phase diagram, this is too low to form rhodium-rich precipitations (Figure 11). Therefore, rhodium dissolves in the β-NiAl phase. The radius of nickel and rhodium atoms is 135 pm,

so rhodium atoms replace nickel atoms in the lattice of the β-NiAl phase and the (Ni,Rh)Al phase is formed. The β-NiAl (atom %: 52.5Al–42.8Ni–4.7Rh) phase was identified in the Ni–Al–Rh alloy after 67 h annealing at 1080 °C [25].

The formation of the rhodium-modified aluminide coating (b) seems to take place in several steps:

(1)   rhodium probably dissolves in γ + γ′ phases near the surface of the CMSX 4 alloy during heating of the alloy with a 0.5 μm rhodium layer at 1040 °C;

(2)   aluminum—during aluminizing in the CVD process—arrives at the surface, where Rh is diluted by Ni. Since aluminum has more affinity to nickel than rhodium, it forms the (Ni,Rh)Al phase layer, similar to the case of the platinum-modified aluminide coating [7]. It is possible that the Rh_xNi_y phase reacts with Al and a (Ni,Rh)Al phase is formed.
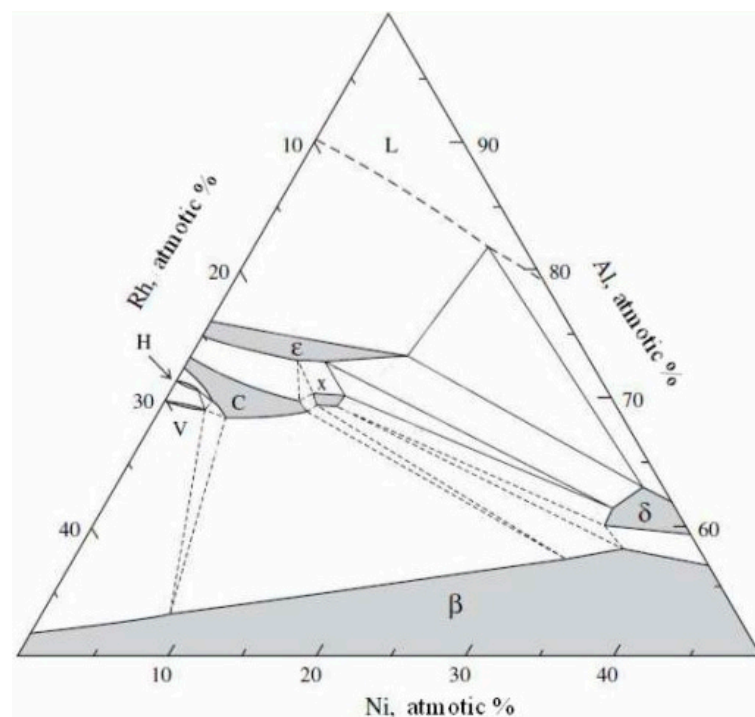
Figure 11. Al–Ni–Rh phase diagram at 1000 °C. Reproduced with permission from [25], published by Elsevier, 2007.

It seems that the (Ni,Rh)Al phase between the additive and interdiffusion layers is formed between the additive and interdiffusion layers in the hafnium- and rhodium-modified aluminide coating (c). The Hf-rich particle distribution at the additive/interdiffusion layer interface indicates that Hf deposition occurs at the beginning of the CVD process. The low hafnium diffusivity and solubility in the β-NiAl is reflected in the distribution of Hf-rich inclusions. They are situated at the additive/interdiffusion layer interface, which corresponds to the initial surface of the substrate. The diffusion activation energy of hafnium is higher than those of rhodium, nickel, and aluminum, but the diffusivity is lower [26]. Therefore, the location of Hf particles remains the same during the coating's growth—only at the additive/interdiffusion layer interface. They do not diffuse to the interdiffusion layer nor to the surface of the coating. Similar results were also obtained by Wang et al. [27]. The Hf solubility limit in the β-NiAl phase is about 0.02 wt % (0.005 atom %) (on pure Ni substrate) or about 0.2 wt % (0.05 atom %) (on NiAl + Hf cast alloys), whereas on Ni-base superalloys it is 0.04–0.15 %wt. higher than on different superalloys [27].

The hafnium addition to the rhodium-modified aluminide coating does not change the coating's formation mechanism. Nevertheless, the low hafnium solubility leads to Hf-rich particle precipitation in the (Ni,Rh)Al phase.

A small rhodium content in aluminide coatings (2–5 atom %) improves the oxidation resistance of the CMSX 4 superalloy. Nevertheless, the rhodium- and hafnium-modified aluminide coating (c) (with small rhodium and hafnium content) has better oxidation resistance than both the rhodium-modified (b) and nonmodified (a) aluminide coatings.

5. Conclusions

Rhodium-modified aluminide coatings were obtained through rhodium (0.5 μm thick layer) electroplating followed by CVD aluminizing. The rhodium- and hafnium-modified aluminide coatings were obtained through rhodium (0.5 μm thick layer) electroplating followed by CVD hafnizing with aluminizing. Nonmodified aluminide coatings were also deposited by CVD aluminizing. The performed investigations proved that:

- The nonmodified (a), rhodium-modified (b), and rhodium- and hafnium-modified (c) aluminide coatings consist of two layers (additive and interdiffusion).
- Rhodium-doped (rhodium- and hafnium-doped) β-NiAl phase was found in the additive layer of the rhodium-modified (rhodium- and hafnium-modified) aluminide coating.
- Rhodium atoms replace nickel atoms in the lattice of the β-NiAl phase, and form the (Ni,Rh)Al phase between the additive and the interdiffusion layers.
- Hf-rich particles precipitate in the (Ni,Rh)Al phase at the additive/interdiffusion layer interface in the rhodium- and hafnium-modified aluminide coating.
- The rhodium-modified aluminide coating (b) has better oxidation resistance than the nonmodified one (a), whereas the rhodium- and hafnium-modified aluminide coating (c) has better oxidation resistance than the rhodium-modified (b) and nonmodified (a) coatings.

Author Contributions: Maryana Zagula-Yavorska conceived, designed the experiments and wrote the paper; Małgorzta Wierzbińska performed the experiments; Jan Sieniawski edited the paper.

Conflicts of Interest: The authors declare no conflict of interest.

References

1. Beranoagirre, A.; Olvera, D.; López de Lacalle, L.N. Milling of gamma titanium–aluminum alloys. *Int. J. Adv. Manuf. Technol.* **2012**, *62*, 83–88. [CrossRef]
2. Shiomi, S.; Miyake, M.; Hirato, T.; Sato, A. Aluminide coatings fabricated on nickel by aluminium electrodeposition from DMSO$_2$-based electrolyte and subsequent annealing. *Mater. Trans.* **2011**, *52*, 1216–1221. [CrossRef]
3. Latief, H.; Sherif, M.; Kakehi, K. Role of aluminide coating on oxidation resistance of Ni-based single crystal superalloy at 900 °C. *Int. J. Electrochem. Sci.* **2015**, *10*, 1873–1882.
4. Latief, H.; Kakehi, K.; Tashiro, Y. Oxidation behavior characteristics of an aluminized Ni-based single crystal superalloy CM186LC between 900 °C and 1100 °C in air. *J. Ind. Eng. Chem.* **2013**, *19*, 1926–1932. [CrossRef]
5. Zhan, Z.; He, Y.; Li, L.; Liu, H.; Dai, Y. Low-temperature formation and oxidation resistance of ultrafine aluminide coatings on Ni-base superalloy. *Surf. Coat. Technol.* **2009**, *203*, 2337–2342. [CrossRef]
6. Lee, J.; Kuo, Y. A study on the microstructure and cyclic oxidation behavior of the pack aluminized Hastelloy X at 1100 °C. *Surf. Coat. Technol.* **2006**, *201*, 3867–3871. [CrossRef]
7. Benoist, J.; Badawi, K.F.; Malie, A.; Ramade, C. Microstructure of Pt-modified aluminide coatings on Ni-based superalloys. *Surf. Coat. Technol.* **2004**, *182*, 14–23. [CrossRef]
8. Purvis, A.; Warnes, B. The effects of platinum concentration on the oxidation resistance of superalloys coated with single-phase platinum aluminide. *Surf. Coat. Technol.* **2001**, *146–147*, 1–6. [CrossRef]

9.   Wang, Y.; Sayre, G. Synthesis of simple and platinum-modified aluminide coatings on cobalt (Co)-base superalloys via a vapor phase aluminizing process. *Surf. Coat. Technol.* **2008**, *203*, 256–263. [CrossRef]
10. Zagula-Yavorska, M.; Sieniawski, J. Microstructural study on oxidation resistance of nonmodified and platinum modified aluminide coating. *J. Mater. Eng. Perform.* **2014**, *23*, 918–926. [CrossRef]
11. Pedraza, F.; Kennedy, A.D.; Koperek, J.; Moretto, P. Investigation of the microstructure of platinum-modified aluminide coatings. *Surf. Coat. Technol.* **2006**, *200*, 4032–4039. [CrossRef]
12. Gleeson, B.; Mu, N.; Hayashi, S. Compositional factors affecting the establishment and maintenance of Al$_2$O$_3$ scales on Ni-Al-Pt systems. *J. Mater. Sci.* **2009**, *4*, 1704–1710. [CrossRef]
13. Koul, A.; Immarigeon, J.; Dainty, R.; Patnaik, P. *Degradation of Advanced Aero Engine Turbine Blades*; ASM International, Materials Park: Geauga County, OH, USA, 1994; Volume 12, p. 69.
14. Haynes, J.A.; Zhang, Y.; Lee, W.Y. *Elevated Temperature Coatings: Science and Technology III*; TMS: Warrendale, PA, USA, 1999; pp. 185–196.
15. Schneider, K.; Arnim, H.; Grünling, H.W. Influence of coatings and hot corrosion on the fatigue behaviour of nickel-based superalloys. *Thin Solid Films* **1981**, *84*, 29–36. [CrossRef]
16. Mu, N.; Izumi, T.; Zhang, L.; Gleeson, B. The development and performance of novel Pt + Hf modified γ'-Ni$_3$Al + γ-Ni bond coatings for advanced thermal barrier coatings systems. *Miner. Met. Mater. Soc.* **2008**, *38*, 629–637.
17. Lee, S.H.; Jun, H.S.; Park, J.H.; Kim, W.; Oh, S.; Park, J.S. Properties of hafnium-aluminum-zinc-oxide thin films for the application of oxide-transistors. *Thin Solid Films* **2016**, *620*, 82–87. [CrossRef]
18. Kim, G.Y.; He, L.M.; Meyer, J.D.; Lee, W.Y.; Quintero, A.; Haynes, J.A. Mechanisms of Hf dopant incorporation during the early stage of chemical vapor deposition aluminide coating growth under continuous doping conditions. *Metall. Mater. Trans. A* **2004**, *35*, 3581–3593. [CrossRef]
19. Felten, E. Use of platinum and rhodium to improve oxide adherence on Ni-8Cr-6Al alloys. *Oxid. Met.* **1976**, *10*, 23–28. [CrossRef]
20. Zagula-Yavorska, M.; Wierzbińska, M.; Gancarczyk, K.; Sieniawski, J. Degradation of nonmodified and rhodium modified aluminide coating deposited on CMSX 4 superalloy. *J. Microsc.* **2016**, *23*, 118–123. [CrossRef] [PubMed]
21. Romanowska, J. Aluminum diffusion in aluminide coatings deposited by the CVD method on pure nickel. *Calphad* **2014**, *44*, 114–118. [CrossRef]
22. Zagula-Yavorska, M.; Sieniawski, J. Cyclic oxidation of palladium modified and nonmodified aluminide coatings deposited on nickel base superalloys. *Arch. Civ. Mech. Eng.* **2018**, *18*, 130–139. [CrossRef]
23. Zagula-Yavorska, M.; Kocurek, P.; Pytel, M.; Sieniawski, J. Oxidation resistance of turbine blades made of ŻS6K superalloy after aluminizing by low-activity CVD and VPA methods. *J. Mater. Eng. Perform.* **2016**, *25*, 1964–1973. [CrossRef]
24. Zagula-Yavorska, M.; Morgiel, J.; Romanowska, J.; Sieniawski, J. Microstructure and oxidation behaviour investigation of rhodium modified aluminide coating deposited on CMSX 4 superalloy. *J. Microsc.* **2016**, *261*, 320–325. [CrossRef] [PubMed]
25. Przepiórzyński, B.; Mi, S.; Grushko, B.; Surowiec, M. An investigation of the Al-Ni-Rh phase diagram between 50 and 100 at% Al. *Intermetallics* **2007**, *15*, 918–928. [CrossRef]
26. Yang, Y.; Jiang, C.; Yao, H.; Bao, Z.; Zhu, S.; Wang, F. Preparation and enhanced oxidation performance of a Hf-dopedsingle-phase Pt-modified aluminide coating. *Corros. Sci.* **2016**, *113*, 17–25. [CrossRef]
27. Wang, Y.; Suneson, M.; Sayre, G. Synthesis of hafnium modified aluminide coatings on Ni-base superalloys. *Surf. Coat. Technol.* **2011**, *15*, 1218–1228. [CrossRef]